Viscous Shock-Layer Solutions around Hypersonic Bodies for Low and High Altitude Flow

S.Ghasemloo[i]; M.Mani[ii]; and M.Malekzade Dirin[iii]

ABSTRACT

An improved method for solving the full viscous shock layer (FVSL) equations for hypersonic flows at low and high altitudes over long slender bodies is presented. This approach can solve both subsonic and supersonic regions of the shock layer without a starting solution for the shock shape and the global iterations are limited only to the nose region. In the nose region (where the subsonic or elliptic flow fields prevails), shock shape is specified from an algebraic expression and corrected through global passes through that region. The shock shape is computed as part of the solution beyond the nose region and requires only a single global pass. Under the high Reynolds number (at low altitudes), the Cebeci-Smith (CS) turbulent model has been analyzed with the present numerical technique for application to long slender bodies. The surface-slip and the currently corrected shock-slip boundary conditions are employed to account for the low-density effects. The method of solution is a spatial-marching, implicit, finite-difference technique, which includes coupling of the normal momentum and continuity equations and uses simple relation instead of Vigneron pressure condition in the subsonic nose region for instability. The results are compared with experimental data and other solutions. The comparisons have been shown to yield accurate results.

KEYWORDS

Aerodynamic Heating, Hypersonic, Viscous Shock Layer .

1. INTRODUCTION

Aerodynamic heating is a major problem associated with all of space missions, and its accurate prediction is critical to the design of hypersonic vehicles. These vehicles are typically slender and the calculation of hypersonic viscous flow fields around the slender axisymmetric blunt bodies are of prime interest to the designer of such re-entry vehicles. Re-entry vehicles operate through a wide range of flow conditions and require the solution to be valid for different Reynolds numbers, from low Reynolds numbers at high altitude to high Reynolds numbers at low altitude.

There are several approaches for treating the problem. The simplest of these approaches is to employ the boundary-layer equations [1]. For relatively large Reynolds numbers the flow field can be devided into an inviscid outer flow and a boundary layer. The classical approach is to solve the inviscid flow field first, and then to use the properties on the body surface as edge conditions for a boundary-layer solutions. Although this approximation is valid for high Reynolds numbers, its accuracy decreases downstream of the nose region of blunt bodies. As the boundary layer grows along the surface, the streamlines which passed the nearly normal portion of the bow shock-wave are swallowed by the boundary layer. Thus, the thick boundary layer and the great entropy gradients in a hypersonic flow make the classical boundary-layer approximation inadequate to predict the flow field. To account for entropy-layer swallowing effects, the boundary layer solution must be coupled with the inviscid flow field solution [2]. Typically in this approach, an inviscid solution to this outer region is

[i] S. Ghasemloo is with the Department of Aerospace Engineering, Amirkabir University of Technology, Tehran, Iran (e-mail: sghasemloo@aut.ac.ir).

[ii] M. Mani is with the Department of Aerospace Engineering and the Center of Excellence in Computational Aerospace Engineering, Amirkabir University of Technology, Tehran, Iran(e-mail: mani@aut.ac.ir).

[iii] Research Assistant, Ph.D, Aerospace Engineering Department .

coupled with a boundary-layer technique. This approach may lead to computational difficulties in the matching procedure on a long body, where strong vorticity interactions occur far downstream. Another approach is to use the Navier-Stokes (NS) equations [3]. This approach successfully provides the solution for the stagnation region of blunt bodies. However, the complexity of the solution procedure due to the elliptic nature of the equations requires excessive computing time and computer storage, which limits their application to short bodies. Thus, it is desirable to reduce the NS equations to a form which can be solved efficiently, while concurrently the physics of the problem is essentially preserved. The methods which have proven successful for the computation of these classes of flow fields are the Parabolized Navier-Stokes (PNS) and Viscous Shock-Layer (VSL) equations [4,5]. The PNS equations can be used to predict many complex three-dimensional, steady, supersonic/hypersonic and viscous flow fields. These equations can be solved using a space marching technique instead of the time marching procedure which is usually employed for the NS equations. They are valid in both viscous and inviscid regions, and thus unlike boundary layer equations no special effort is needed for viscous/inviscid interactions. The principle difficulty in applying the PNS equations to the hypersonic vehicles is that commonly the algorithms cannot solve blunt-body flow fields, while most re-entry vehicle designs incorporate blunted nose in order to reduce peak heating rates. In addition, the numerical solution of the PNS equations requires a substantial amount of computer time and storage.

The third approach is to employ the viscous shock-layer (VSL) equations. The VSL equations are a subset of the NS equations and are obtained by retaining terms up to second order in the inverse square root of the Reynolds number. The VSL equations were developed by Davis [5] and yield a simplified set of governing equations that are uniformly valid through the shock layer to moderately low Reynolds numbers [6]. The VSL equations are of mixed hyperbolie elliptic in the subsonic nose region of a blunt body and are of mixed hyperbolic-parabolic type in the streamwise direction where the flow becomes supersonic. The streamwise gradients of pressure and normal velocity cause the VSL equations to be elliptic in the subsonic nose region. Moreover, the effects of the unknown shock shape is to introduce an elliptic type behavior[7].

The VSL method can accurately predict the blunt-body flow field for a small fraction of the computing time required by NS schemes. This choice is very desirable for the preliminary design process where a range of geometries and flow parameters must be analyzed. The VSL method has been shown to provide results in good agreement with experimental data and results of other methods [8-10]. Numerous computational schemes for the solution of the viscous shock-layer equations have been investigated in the past. Davis [5] presented an implicit finite-difference method to solve the VSL equations for a wide-angle body (45-deg hyperboloid). Davis [5] obtained a first global solution using the thin viscous shock layer (TVSL) assumption, the elliptic nature was then satisfied with subsequent global iterations. The main difficulties with the method of Ref. [5] were identified as the shock shape divergence problem and the slow convergence. Werle et al. [11] developed an Alternating Direction Implicit (ADI) technique with an artificial time coordinate to relax the shock shape from an initial shape. Even with this relaxation scheme, the instabilities were encountered with long, slender blunt bodies (where the inviscid region in the far downstream encompasses a significant portion of the total shock layer). Hosney et al. [12] and Gordon and Davis [7] have solved the governing equations as a fully coupled set. Coupling the equation for shock standoff distance does result in a convergence problem in Ref. [7]. A relaxation scheme is used there for updating the shock standoff distance after each global pass, and the first streamwise derivative of the shock standoff distance is taken from the previous global iteration to overcome the convergence problem. In these methods, computational time and the storage and computing requirements are quite large. Waskiewicz et al. [13] introduced the more adequate method. In Ref.[13] the normal and global continuity equations were solved simultaneously for the pressure and normal velocity. Some papers basically followed this method and successfully implemented for blunt bodies [14]-[16].

In the previous papers, an initial shock shape was required to start the solution of VSL equations. Moreover, the shock shape extending to the entire length of the body is globally iterated. The initial shock shape generation and the global iterations over the entire length of the body requiring considerable computational effort and run time respectively. For a slender body, Gupta et al. [6,17] successively relaxed the shock shape from a wide-angle body to a slender body. In other words, in the approach of Ref. [6,17], the initial shock shape is created by the thin viscous shock layer approximation for a short, wide-angle body (35-deg sphere cone, for example). The shock shape obtained from a full viscous shock layer solution to this body in a sequential manner by reducing the body angles in steps of 5 to 10 deg. Also, to reduce run time, the shock shape extending to a location beyond the shock-inflection point (shock recompression zone) is globally iterated. However, since this zone persists over an extensive region for smaller body angles, limiting the global iterations only through the shock recompression zone may still require considerable computational time.

The present approach generates its own shock shape as a part of solution and provide a smooth shock shape in subsonic and supersonic regions. Therefore, the input shock shape obtained from a different solution is not required. It eliminates the need for initial shock shape, which was required by previous methods of solutions.

Moreover, the global iterations are limited to the subsonic region which is small region in the hypersonic flow over the blunt bodies. In addition, the solution of thin viscous shock layer equations is not required to solve the full VSL equations as was done in Refs. [5] and [18]. The VSL equations in this paper are solved in a shock oriented (rather than the traditional body oriented) coordinate system. Note that the use of a body coordinate system introduces discontinuities in the solution of governing equations associated with the surface curvature discontinuity, such as at the sphere-cone tangency point of a spherically blunted cone [18]. In the present work, shock oriented coordinate is used and the shock shape is described by an analytical equation, so the curvature derivative is well-behaved and the pressure gradient can be evaluated analytically. The difficulties related to juncture point are omitted, too. In this paper, the Cebeci-Smith (CS) turbulence model is implemented to predict turbulence effects.

The low-density flow conditions are important to understand since the aerospace vehicle aerodynamics can significantly be influenced. In this investigation, the surface-slip and shock-slip conditions are employed to obtain the results for the low-density flight conditions.

2. ANALYSIS

A brief discussion of the flow governing equations, the boundary conditions and method of solution are presented in the following analysis.

2.1 Governing Equations

The conservation equations employed in this analysis are the steady, viscous shock-layer equations for an axisymmetric body at zero angle of attack. These equations are developed in a shock-oriented coordinate system (s,n) where the s coordinate is tangent to the shock in the streamwise direction and n is the coordinate normal to the shock (see Fig. 1).To facilitate the solution, the VSL equations are transformed to normalized coordinates (ξ,η_n).The nondimensional forms of the VSL equations in a normalized shock-oriented coordinate system are:

Continuity Eq.

$$\frac{\partial}{\partial\xi}(\rho u h_3)-\frac{\eta_n-1}{n_b}\frac{dn_b}{d\xi}\frac{\partial}{\partial\eta_n}(\rho u h_3)-\frac{1}{n_b}\frac{\partial}{\partial\eta_n}(\rho v h_1 h_3)=0 \qquad (1)$$

n-momentum Eq.

$$\rho[\frac{u}{h_1}\frac{\partial v}{\partial\xi}-(\frac{v}{n_b}+\frac{u}{h_1}\frac{\eta_n-1}{n_b}\frac{dn_b}{d\xi})\frac{\partial v}{\partial\eta_n}+\frac{u^2}{h_1 n_b}\frac{\partial h_1}{\partial\eta_n}]-\frac{1}{n_b}\frac{\partial p}{\partial\eta_n}=0 \qquad (2)$$

s-momentum Eq.

$$\rho[\frac{u}{h_1}(\frac{\partial u}{\partial\xi}\frac{\eta_n-1}{n_b}\frac{dn_b}{d\xi}\frac{\partial u}{\partial\eta_n})-\frac{v}{n_b}(\frac{\partial u}{\partial\eta_n}+\frac{u}{h_1}\frac{\partial h_1}{\partial\eta_n})]+\frac{1}{h_1}(\frac{\partial P}{\partial\xi}\frac{\eta_n-1}{n_b}\frac{dn_b}{d\xi}\frac{\partial u}{\partial\eta_n})=$$

$$\frac{\varepsilon^2}{n_b^2}\left\{\frac{\partial}{\partial\eta_n}[\mu(1+\varepsilon^+)\frac{\partial u}{\partial\eta_n}-\mu\frac{u}{h_1}\frac{\partial h_1}{\partial\eta_n}]+(\frac{2}{h_1}\frac{\partial h_1}{\partial\eta_n}+\frac{1}{h_3}\frac{\partial h_3}{\partial\eta_n})[\mu(1+\varepsilon^+)\frac{\partial u}{\partial\eta_n}-\mu\frac{u}{h_1}\frac{\partial h_1}{\partial\eta_n}]\right\} \qquad (3)$$

Energy Eq.

$$\rho[\frac{u}{h_1}(\frac{\partial h}{\partial\xi}-\frac{\eta_n-1}{n_b}\frac{dn_b}{d\xi}\frac{\partial h}{\partial\eta_n})-\frac{v}{n_b}\frac{\partial h}{\partial\eta_n}]-\frac{u}{h_1}[\frac{\partial p}{\partial\xi}-\frac{\eta_n-1}{n_b}\frac{dn_b}{d\xi}\frac{\partial p}{\partial\eta_n}]+\frac{v}{n_b}\frac{\partial p}{\partial\eta_n}$$

$$=\frac{\varepsilon^2}{n_b^2}\left\{\frac{\partial}{\partial\eta_n}[\frac{\mu}{\mathrm{Pr}}(1+\varepsilon^+\frac{\mathrm{Pr}}{\mathrm{Pr}_t})\frac{\partial h}{\partial\eta_n}]+\frac{\mu}{\mathrm{Pr}}(1+\varepsilon^+\frac{\mathrm{Pr}}{\mathrm{Pr}_t})(\frac{1}{h_1}\frac{\partial h_1}{\partial\eta_n}+\frac{1}{h_3}\frac{\partial h_3}{\partial\eta_n})\frac{\partial h}{\partial\eta_n}\right.$$

$$\left.+[\mu(1+\varepsilon^+)\left\{(\frac{\partial u}{\partial\eta_n})^2-2\frac{u}{h_1}\frac{\partial h_1}{\partial\eta_n}\frac{\partial u}{\partial\eta_n}\right\}+\mu(\frac{u}{h_1}\frac{\partial h_1}{\partial\eta_n})^2]\right\} \qquad (4)$$

State Eq.

$$p=\rho T\frac{\gamma-1}{\gamma} \qquad (5)$$

In the transformed coordinate system employed here, the metrics are:

$$h_1=1+n_b(\eta_n-1)\kappa_{sh} \qquad h_3=r_{sh}+n_b(\eta_n-1)\cos\Gamma_{sh}$$

In this study, the molecular and turbulent Prandtl numbers are assumed to be 0.72 and 0.9, respectively. Sutherland relation is employed to calculate the viscosity.

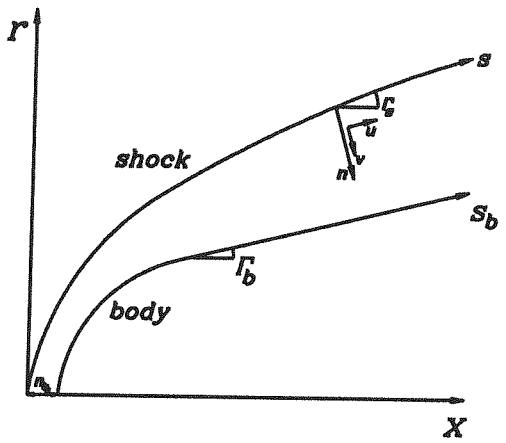

Figure 1: Shock-oriented coordinate system.

2.2 Boundary Conditions

At low altitudes, slip effects are not important, so the no slip condition (u=v=0) is applied at the wall. In addition, the wall temperature and enthalpy are specified constant. The shock jump conditions are given by the Rankin-Huguenot relations [5].

At high altitudes, the no-slip boundary conditions are no longer valid. The density decreases at higher altitudes, so the continuum flow equations that describe the flow adequately under high Reynolds number flow conditions are no longer adequate near the wall. The flow in a region next to the wall having a thickness on the order of a local mean free path (the Knudsen layer) cannot be analyzed through the continuum description because there are insufficient collisions for this description to be valid. Also, it is known that as the Reynolds number decreases in hypersonic flow, the thickness of shock wave increases such that the Rankine-Hugoniot discrete shock relations become inadequate. Therefore, the slip and temperature jump boundary conditions should be used. The relations for the surface and shock slip conditions are provided in the following.

2.2.1 Surface Conditions

Under low Reynolds number high-altitude flight conditions , the density at the surface of a space vehicle is sufficiently low so that the velocity, temperature, and

pressure at the wall are no longer the same as those of the gas adjacent to the wall. This difference in the values of various quantities is known as "surface slip," and the equations describing this phenomena are known as surface-slip equations. These equations play an important role in the accurate prediction of aerothermal environment of space vehicles entering the Earth's atmosphere. In this paper, the surface slip condition for a single-species gas as given by Gupta et al.[19] are used as the boundary conditions on the body surface. The nondimensional forms of surface-slip conditions in the transformed coordinate system are given as:

velocity slip condition :

$$u_s = \sqrt{\frac{\pi}{2}}\frac{2-\theta}{\theta}\frac{\varepsilon^2\mu_s}{\sqrt{p_s\rho_s}}[(\frac{1}{n_b}\cos(\Gamma_{sh}-\Gamma_b)-\frac{\eta_n-1}{n_b}\frac{dn_b}{d\xi}\times$$

$$\sin(\Gamma_{sh}-\Gamma_b))\frac{\partial u}{\partial\eta_n}+\sin(\Gamma_{sh}-\Gamma_b)\frac{\partial u}{\partial\xi}+\frac{\kappa_{sh}u}{1+(\eta_n-1)n_b\kappa_{sh}}]_s \quad (6)$$

pressure slip condition :

$$P_s = P_w+\frac{4}{5\sqrt{2\pi}}(\frac{\gamma}{\gamma-1})(\frac{2-\theta}{\theta})\frac{\epsilon^2}{\Pr}\frac{\mu_S}{T_s}\sqrt{\frac{P_s}{\rho_s}}[(\frac{1}{n_b}\cos(\Gamma_{sh}-\Gamma_b)$$

$$-\frac{\eta_n-1}{n_b}\frac{dn_b}{d\xi}\sin(\Gamma_{sh}-\Gamma_b))\frac{\partial T}{\partial\eta_n}+\sin(\Gamma_{sh}-\Gamma_b)\frac{\partial T}{\partial\xi}]_s \quad (7)$$

temperature slip condition :

$$T_s = T_w+\frac{1}{2}\sqrt{\frac{\pi}{2}}(\frac{\gamma}{\gamma-1})(\frac{2-\theta}{\theta})\frac{\varepsilon^2}{\Pr}\frac{\mu_s}{\sqrt{p_s}}[(\frac{1}{n_b}\cos(\Gamma_{sh}-\Gamma_b)$$

$$-\frac{\eta_n-1}{n_b}\frac{dn_b}{d\xi}\sin(\Gamma_{sh}-\Gamma_b))\frac{\partial T}{\partial\eta_n}+\sin(\Gamma_{sh}-\Gamma_b)\frac{\partial T}{\partial\xi}]_s \quad (8)$$

2.2.2 *Shock Conditions*

The shock slip conditions are the modified Rankin-Hugoniot relations, which are obtained from the integration of one-dimensional Nervier-Stokes equations through the shock transition zone. The integration is carried out from the interface behind the shock transition zone (where the usual Rankin-Hugoniot shock relations apply) to free stream. The nondimensional forms of shock conditions[5] in the transformed coordinate system are expressed as:

Continuity

$$\rho_{sh}v_{sh} = \sin\Gamma_{sh} \quad (9)$$

s-momentum

$$-\frac{\varepsilon^2\mu_{sh}}{n_b}(\frac{\partial u}{\partial\eta_n})_{sh}+u_{sh}\sin\Gamma_{sh} = \sin\Gamma_{sh}\cos\Gamma_{sh} \quad (10)$$

n-momentum:

$$p_{sh} = p_\infty+\sin\Gamma_{sh}(\sin\Gamma_{sh}-v_{sh}) \quad (11)$$

Energy:

$$-\frac{\varepsilon^2\mu_S}{P_r}(\frac{1}{n_b}\frac{\partial T}{\partial\eta_n})_{sh}+T_{sh}\sin\Gamma_{sh}-\frac{\sin\Gamma_{sh}}{2}(u_{sh}-\cos\Gamma_{sh})^2 = \frac{\sin\Gamma_{sh}}{2}\times$$

$$\left\{\frac{4\gamma}{(\gamma+1)^2}\sin^2\Gamma_{sh}+\frac{1}{M_\infty^2}[(\frac{2}{\gamma-1})-\frac{4(\gamma-1)}{(\gamma+1)^2}]-\frac{4}{(\gamma+1)^2M_\infty^4\sin^2\Gamma_{sh}}\right\} \quad (12)$$

2.3 *Shock Shape*

The full VSL equations require an initial shock shape for the first global iteration. The shock shape obtained in the first iteration solution is used as the input shape for a second iteration. This procedure is repeated until the new calculated shock shape varies little from the input shape. Most of existing VSL schemes use the various procedures (thin viscous shock layer, inviscid solution,...) to obtain an initial shock shape. However, obtaining the initial shock shape from these procedures require considerable computational effort.

In the solution procedure used by Davis [5] and Moss [20] , a first global solution was obtained using the thin viscous shock layer(TVSL) assumption. The TVSL approximation, however, fails for slender bodies with cone angles less than about 30 degree. In Refs.[15] and [21], the initial shock shape is obtained from an Euler code. In the approach of Ref.[17], a catalog of shock shapes is created by starting from a large body angle (with TVSL approximation) through sequential reduction in the body angles. One has to store these shock shapes for use in a problem with approximately the same body angle.

In the present approach, the shock shape is generated as part of the solution. The shock shape is calculated based upon the method which is presented in Ref. [22]. As mentioned earlier, the subsonic-transonic region is elliptic in nature, therefore, a marching scheme is not well posed. Thus, the complete shock shape for the entire subsonic-transonic region must be determined iteratively. A marching procedure is then used downstream of the subsonic-transonic region where the inviscid layer is supersonic. Generally, the three-dimensional shock surface in the subsonic-transonic can be represented by three longitudinal conic sections blended in the circumferential direction with an ellipse as:

$$r = f(x,\phi) \quad (13)$$

where $f(x,\phi)$ is defined as

$$f^2\left[B(x)\cos^2(\phi)+\sin^2(\phi)\right]+fC(x)\cos(\phi) = D(x) \quad (14)$$

in which

$$B(x) = \frac{f_2^2}{f_1 f_3}$$

$$C(x) = B(x)(f_3-f_1)$$

$$D(x) = f_2^2$$

Note that F(x,ϕ) is the radial coordinate of the 3D shock surface in shock cylindrical coordinate system. The equation of the longitudinal conic sections is given by

$$f_k^2+b_kx^2-2c_kx+2d_kxf_k = 0 \quad ,k=1,2,3 \quad (15)$$

where k represents shock profiles for ϕ=0°, 90° and 180°, respectively. The shock shape, defined above includes nine parameters of b_k, c_k and d_k where K=1,2,3. For an axisymmetric flow, the total number of parameters governing the shock surface is reduced to b_1 and c_1 [22]. The quantities b_1 and c_1 are determined through a quasi-Newton iterative procedure. With each variation of these two parameters, the flowfield is solved for the entire subsonic region. The values for the calculated shock layer thickness at two stations near the end of the subsonic region are compared with the values dictated by the

geometry. Shock iterations are continued until the calculated values of n_b at these two stations match the geometric values. Downstream the subsonic-transonic region, the initial shock shape is calculated by linear extrapolation of previous values and is corrected iteratively using the secant method. It is noted that the shock shape convergence is achieved with four to six iterations per station. The shock shape for the supersonic region is described by:

$$r = r_{i-1} + \Delta x \frac{dr}{dx}|_{i-1} + \frac{\Delta x^2}{6}[2\frac{d^2r}{dx^2}|_{i-1} + \frac{d^2r}{dx^2}|_i] \quad (16)$$

where the shock derivative is given by

$$\frac{dr}{dx} = \frac{dr}{dx}|_{i-1} + \frac{\Delta x}{2}[\frac{d^2r}{dx^2}|_{i-1} + \frac{d^2r}{dx^2}|_i] \quad (17)$$

The only unknown in Eqs.16 and 17 is the second derivative of r with respect to the x which is proportional to the shock curvature at the current station. As an initial value, the curvature at station i is extrapolated from its values at the previous two stations. Once the shock geometry and the corresponding jump conditions are constrained, the governing equations are solved. Then the calculated and geometric values of n_b are compared to determine the error (δerr). Through successive application of the secant method (accompanied by a solution to the fluid equations), δerr converges to a specified tolerance. In summary, in the subsonic-transonic region, shock shape is specified from an algebraic relation and corrected through global iterations through that region. The shock shape is computed as part of the solution beyond the subsonic-transonic region. Thus, shock shape is not required as an input by the user.

3. METHOD OF SOLUTION

The method used for solving the full VSL equations is a spatial-marching, implicit, finite-difference method which includes coupling of the continuity and normal momentum equations. In the normalized shock-coordinate system (ξ,ηn), the conservation equation for streamwise momentum and energy can be written in the standard parabolic form :

$$A_0 \frac{\partial^2 W}{\partial \eta_n^2} + A_1 \frac{\partial W}{\partial \eta_n} + A_2 W + A_3 + A_4 \frac{\partial W}{\partial \xi} = 0 \quad (18)$$

where W represents the dependents variables u and h, respectively. The coefficients A_0 through A_4 are nonlinear coefficients. For the energy equation, the nonlinearities are handled through a simple lagging technique. However, in order to speed up convergence, the streamwise momentum equation is quasi-lineralized. In the finite-difference method used to solve the streamwise and energy equations, a two point backward differences is used for the derivatives with respect to ξ. The derivatives with respect to the η_n are replaced with three-point central differences. Replacing the differential terms by the finite-difference expressions, the governing equations are expressed as:

$$A_j W_{i,j-1} + B_j W_{i,j} + C_j W_{i,j+1} = D_j \quad (19)$$

Evaluating the coefficients of Eq. (19) at discrete points across the shock layer along with the boundary conditions yields a tri-diagonal system of equations which may be solved using Thomas algorithm. The continuity and normal momentum equations are first order differential equations and, when solved independently, pose numerical difficulties. However, using the coupling approach, these two first equations are coupled together to form a second-order system that can be solved using Thomas algorithm. These equations are solved for the pressure and normal velocity. The density in these equations is eliminated by using the equation of state. The resulting equations are expressed in the finite-difference form at points $(i, j+\frac{1}{2})$ and $(i, j-\frac{1}{2})$ using a box scheme. The final form for the continuity equation are :

$$A_{c,j+\frac{1}{2}} V_{i,j+1} + B_{c,j+\frac{1}{2}} V_{i,j} + C_{c,j+\frac{1}{2}} P_{i,j+1} + D_{c,j+\frac{1}{2}} P_{i,j} = E_{c,j+\frac{1}{2}} \quad (20)$$

$$A_{c,j-\frac{1}{2}} V_{i,j} + B_{c,j-\frac{1}{2}} V_{i,j-1} + C_{c,j-\frac{1}{2}} P_{i,j+1} + D_{c,j-\frac{1}{2}} P_{i,j-1} = E_{c,j-\frac{1}{2}}$$

$$A_{nm,j+\frac{1}{2}} V_{i,j+1} + B_{nm,j+\frac{1}{2}} V_{i,j} + C_{nm,j+\frac{1}{2}} P_{i,j+1} + D_{nm,j+\frac{1}{2}} P_{i,j} = E_{nm,j+\frac{1}{2}}$$

$$A_{nm,j-\frac{1}{2}} V_{i,j} + B_{nm,j-\frac{1}{2}} V_{i,j-1} + C_{nm,j-\frac{1}{2}} P_{i,j} + D_{nm,j-\frac{1}{2}} P_{i,j-1} = E_{nm,j-\frac{1}{2}}$$

The coefficients of these equations are given in the Appendix. Eliminating p and v alternatively in the coupled equations, two tridiagonal equations for pressure and normal velocity are obtained as:

$$A_p P_{i,j-1} + B_p P_{i,j} + C_p P_{i,j+1} = D_p \quad (21)$$

$$A_v V_{i,j-1} + B_v V_{i,j} + C_v V_{i,j+1} = D_v \quad (22)$$

Equations (21) and (22) are solved in the same way as the streamwise momentum and energy equations. This numerical coupling enhances considerably the overall numerical stability of the VSL solution scheme. Note that the shock standoff distance is evaluated by integrating the continuity equation.

Cebesi-Smith(CS) [23] turbulence model is implemented in the present method to predict turbulence effects. The boundary layer edge location is required in the CS model and there are some criterion for obtaining the boundary layer thickness. In the present work, the boundary layer thickness is assumed to be the value of η_n at point where:

$$\frac{d(H/H_\infty)}{d\eta_n} \le 0.5 \quad (23)$$

In the laminar to turbulent transition region, the composite eddy viscosity ε+ is modified using the Dhawn and Narashima method [24]. For the laminar flow and slip-conditions, the eddy viscosity is set to zero. Maslen's relation [22] is used for the pressure gradient in the streamwise momentum and energy equations in the subsonic nose region. The pressure gradient can be evaluated analytically because the shock shape is described analytically. Differentiating Maslen's relation with respect to η_n gives.

$$\frac{\partial p}{\partial \xi}\Big|_{\eta_n} = [\frac{(1-\eta)v_{sh}}{2n_b \cos\Gamma_{sh}}(1-\frac{\kappa_{sh} r_{sh}}{\cos\Gamma_{sh}}) + \frac{\eta_n - 1}{n_b}\frac{dn_b}{d\xi}]\frac{\partial P}{\partial \eta_n} + \frac{\partial P}{\partial \xi}\Big|_{\eta} \qquad (24)$$

Note that the above relation is a function of η and the relation between η and η_n can be derived from the continuity equation. In this paper, this relation is given by:

$$\eta = \frac{2\rho_{sh} u_{sh} h_3}{r_{sh}^2} n_b (\eta_n^3 - \eta_n) - 2\eta_n^3 + 3\eta_n^2 \qquad (25)$$

The derivation of equation (25) is described in detail in Ref.[25] and, hence, is not discussed here.

The solution is started at the stagnation line. The flowfield along the stagnation line involves a removable singularity that can be removed by using an explicit limiting form of the governing equations [26]. This approach yields a set of ordinary differential equations. Using the stagnation line solution, the VSL equations are solved at the next down stream location by employing a two point backward-difference approximation for the streamwise derivative. The solution is iterated until it converges. This procedure is repeated until a global solution at all locations is obtained. It is mentioned that at each location the equations are solved in the following order: 1)energy, 2) streamwise momentum, 3) integration of continuity for n_b, 4) solving the continuity and normal momentum equations simultaneously for p and v 5) solving the equation of state for p.

4. Result and Discussion

Numerical solutions of the viscous shock-layer (VSL) equations with the present method for the high and low Reynolds number hypersonic flow over long slender bodies are obtained. Results are for the laminar, transitional, and turbulent flow over slender bodies. The accuracy of these results is demonstrated by comparisons with the experimental data and other predictions. The surface and shock slip boundary conditions are implemented in the present method to obtain results for the low-density (high altitudes) flight condition. At the wall, although both variable temperature and constant temperature conditions can be imposed, in the present work only the constant wall temperature condition is considered.

In Figs. 2 to 3, the laminar heating results from the present method are compared with experimental data. Figure 2 presents laminar heating rates over a blunted 15-deg cone at a freestream Mach number of 10.6 for nose radius of 0.009525m and 0.02794m. It can be seen that the results from the present method is in good agreement with the experimental data [27]. Figure 2 also illustrates the blandness effect problem. It can be seen, as is expected, the heating rate for R_n=0.02794m nose is dramatically less than that for 0.009525m. In Fig. 3, the data were measured over a blunted 12.84-deg cone at a freestream Mach number of 10.16 and the surface heat transfer rate agrees excellently with the experimental values of Miller [28]. The results obtained by the present viscous shock-layer (VSL) are compared with parabolized Navier-Stokes(PNS) predictions [29] for a long 5-deg sphere cone in Fig. 4. The VSL results are about 5-12% lower for most of the body length as compared to the PNS

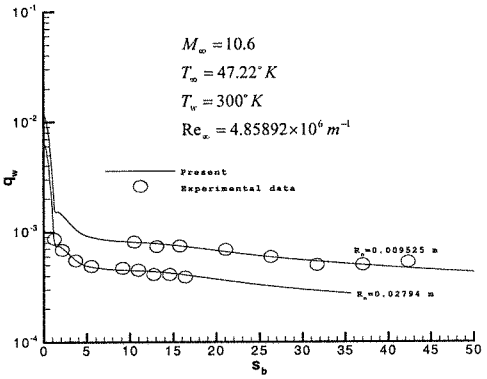

Figure 2: Heat transfer comparison for 15 (deg) sphere-cone with laminar flow.

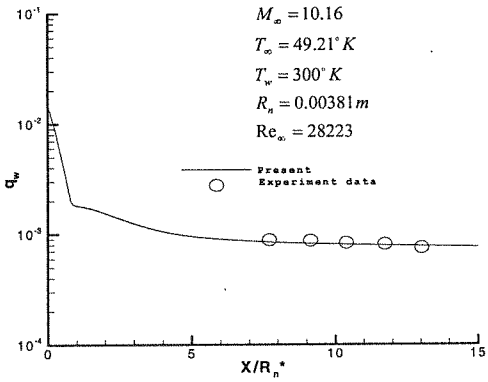

Figure 3:Heat transfer comparison for 12.85 (deg) sphere-cone with laminar flow.

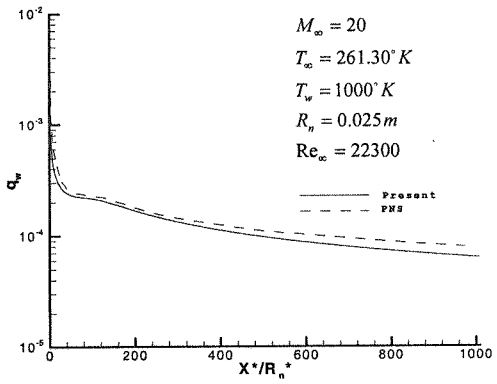

Figure 4: Surface heat transfer rate distribution for a 5 (deg) sphere-cone with laminar flow.

results. The PNS predictions employ fourth-order explicit and second-order implicit smoothing terms, whereas the present VSL calculations do not use any smoothing. Furthermore, the stability of PNS solutions restricts the reduction of the normal grid spacing adjacent to the wall (required for accurate heat transfer predictions) if a relatively large marching step size is required for a long body. Since the PNS requires a starting solution that

describes the subsonic region, any starting solution errors distort the PNS results in the nose region. In the VSL, the starting profiles are created as a part of solution and, thus,

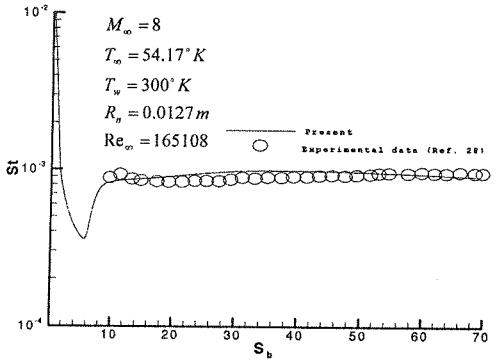

Figure 5: Stanton number distribution for a 7 (deg) sphere cone with turbulent flow.

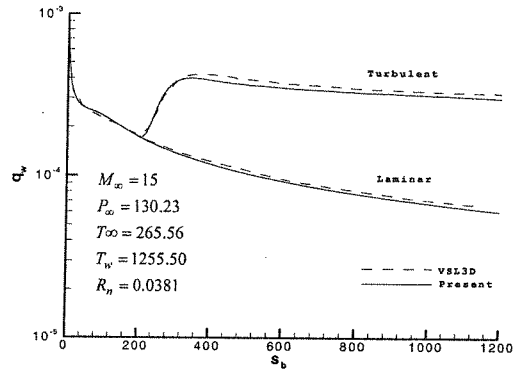

Figure 6: Surface heat transfer rate distribution for a 5 (deg) sphere-cone.

the method is self starting.

The results for the turbulent flow are illustrated in Figures 5 and 6. Cebesi-Smith turbulence model is implemented in the present method to predict turbulence effects. The definition of the boundary edge is based on the gradient of the total enthalpy [Eq.(23)]. The results for the Stanton number distributions for a 7-deg sphere cone are given in Fig. 5. The transition to turbulence is initialized at S_b =4.8 as given by the data of Carver [30]. In Figure 5, the heating results from the present method are seen to compare well (generally within 10 percent) with the experimental data [30]. In Figure 6, the computed heating from the present method and the VSL3D method [15] are presented for a 5-deg blunt Cone at a Mach number of 15. The results of laminar and turbulent flow calculations are shown in this Figure. The transition point is specified to be at S_b=192. The laminar results of VSL3D and present method are in good agreement (within 7%) and the turbulent results of the present method are approximately 5-12% lower than VSL3D values.Results at low Reynolds number conditions have been presented in Figs 7 to 9. At high altitudes, the assumption of a continuum flow becomes tenuous and the no-slip boundary conditions are no longer valid. As such, the slip boundary conditions should be used. The low-density effects are characterized

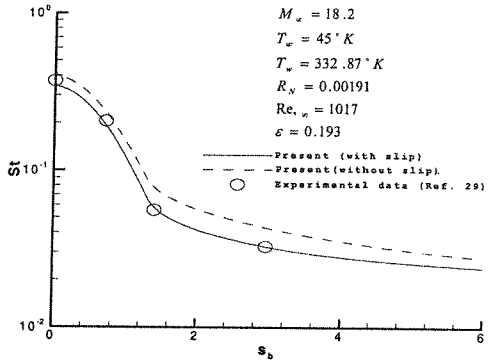

Figure 7: Stanton number distribution for a 10 (deg) sphere-cone with ε =0.194.

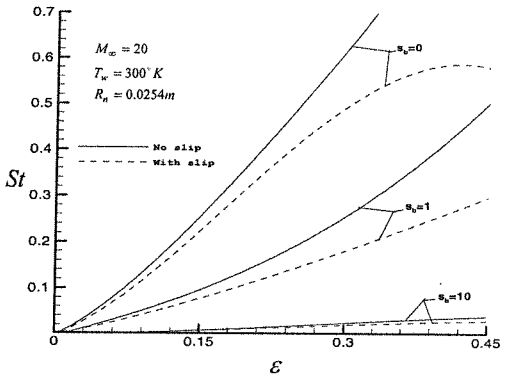

Figure 8: Stanton number distribution for a 5 (deg) sphere cone as a function of ε.

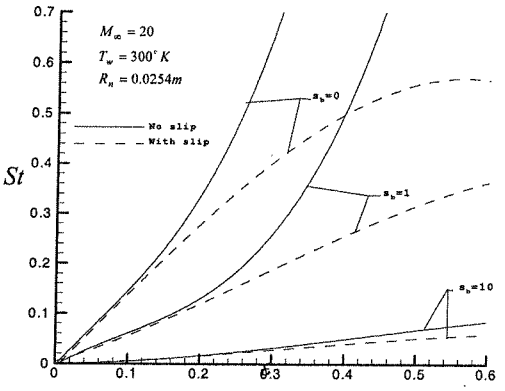

Figure 9: Stanton number distribution for a 10 (deg) sphere cone as a function of ε.

by the Reynolds-number parameter [5], ε, and become generally significant for values of ε greater than about 0.1. Results obtained for a 10-deg sphere-cone and ε=0.193 by the present method are compared with the heat transfer data of Boylan [31] in Fig. 7. The present calculations with slip conditions are in good agreement with the data of Boylan. Using the slip boundary conditions decreases the heat transfer rate and improves the agreement of the VSL predictions with the experimental data. Figures 8 and 9

show the effect of cone angle with slip boundary conditions. Results have been calculated for five and ten degree sphere cones, 0.0254 nose radius and high Mach number flow (M∞=20) over highly cooled surface (Tw=300K). According to Figs. 8 and 9, increasing in ε or altitude causes slip effect to be increased. Furthermore for great S_b, its effect is insignificant. These Figures also show that the heat transfer rates for ε less than 0.1 are the same for slip and no-slip Conditions, therefore, the slip conditions should be used for ε greater than 0.1. Figure 9 illustrates that the Stanton number values for a 10-deg sphere-cone are higher than those for a 5-deg sphere-cone at the corresponding body locations for a given Reynolds-parameter (or altitudes). This result is valid for both cases of with and without slip condition. Finally, Figure 8 and 9 indicate that the largest slip effects occur in the nose region.

5. Conclusions

A new technique to solve VSL equations is proposed with increases computational efficiency. In the present method, initial shock shape is not required and the global iteration is confined merely to nose region. The shock shape is defined with an algebraic (conic) equation and is iterated globally in the nose region till the calculated body matches with the real body at the end of the subsonic region. In the supersonic region, the marching scheme is well posed. Hence, the shock shape and flow field can be determined in each station and there is no need for global iteration. In previous methods [7,16,17] Vigneron's relations were used for subsonic region for stability and convergence. However, using this relation requires an initial flow field solution. In the present work, a relation for pressure gradient in the streamwise direction is derived using the Maslen's equation and is used instead of Vigneron's relation for stability of numerical solution. In supersonic region the pressure gradient can be calculated readily and there is no need for the above relation. Since the subsonic region is only a small portion of the flow field for hypersonic flows over slender bodies, and the global iteration is confined for this region only in the present method, a dramatic reduction in CPU time is achieved. Moreover, the shock shape is described in three dimensions that makes this technique extendable to three dimensional flows. Moreover, by using the shock coordinated systems the junction point problem in sphere-cone configurations is solved. The Cebeci-Smith (CS) model has been used to define eddy viscosity in the present work. The obtained results from the present method show that the CS model adequate for turbulent flows. In the laminar to turbulent transition region, the composite eddy viscosity is modified using the Dhawan and Narashima method [22]. Under the low density flow condition, the surface and shock slip conditions have been implemented in the present VSL method for a perfect gas. Results of the present method compare quite favorably with experimental data and other predictions. In conclusion, a wide range of flow conditions have been considered and a method for analyzing the flow is demonstrated.

6. Appendix

The coefficients for Equations (20) are obtained as follows:

$$A_{c,j+1/2} = -\frac{(h_1 h_3)_{j+1/2}}{\Delta\eta_{n,j+1}}$$

$$B_{c,j+1/2} = \frac{(h_1 h_3)_{j+1/2}}{\Delta\eta_{n,j+1}}$$

$$C_{c,j+1/2} = \frac{n_b h_{3,j+1/2} u_{i,j+1/2}}{2\Delta\xi_i P_{i,j+1/2}} - \frac{1}{\Delta\eta_{n,j+1} P_{i,j+1/2}}\left[\frac{dn_b}{d\xi}\frac{h_{3,j+1/2}(\eta_{n,j+1/2}-1)}{1} + (h_1 h_3)_{j+1/2} V_{i,j+1/2}\right]$$

$$D_{c,j+1/2} = \frac{n_b h_{3,j+1/2} u_{i,j+1/2}}{2\Delta\xi_i P_{i,j+1/2}} + \frac{1}{\Delta\eta_{n,j+1} P_{i,j+1/2}}\left[\frac{dn_b}{d\xi}\frac{h_{3,j+1/2}(\eta_{n,j+1/2}-1)}{1} + (h_1 h_3)_{j+1/2} V_{i,j+1/2}\right]$$

$$E_{c,j+1/2} = \frac{n_b h_{3,j+1/2} u_{i,j+1/2}}{2\Delta\xi_i P_{i,j+1/2}}(P_{i-1,j+1} + P_{i-1,j}) - \frac{n_b h_{3,j+1/2}}{2\Delta\xi_i}(u_{i,j+1} + u_{i,j} - u_{i-1,j} - \frac{u_{i,j+1/2}}{T_{i,j+1/2}} \times$$

$$(T_{i,j+1} + T_{i,j} - T_{i-1,j+1} - T_{i-1,j})) - \frac{n_b u_{i,j+1/2}}{2\Delta\xi_i}((h_3)_{i,j+1} + (h_3)_{i,j-1} - (h_3)_{i-1,j+1} - (h_3)_{i-1,j})$$

$$+ V_{i,j+1/2} * \left[(h_1)_{j+1/2}(\frac{\partial h_3}{\partial \eta_n})_{j+1/2} + (h_3)_{j+1/2}(\frac{\partial h_1}{\partial \eta_n})_{j+1/2}\right] - \frac{V_{i,j+1/2}(h_1 h_3)_{j+1/2}}{\Delta\eta_{n,j+1} T_{i,j+1/2}}[T_{i,j+1} - T_{i,j}]$$

$$+ \frac{n_b h_{3,j+1/2}(\eta_{n,j+1/2}-1)}{\Delta\eta_{n,j+1}}\left[u_{i,j+1} - u_{i,j} - \frac{u_{i,j+1/2}}{T_{i,j+1/2}}(T_{i,j+1} - T_{i,j})\right]$$

$$A_{NM,j+1/2} = \frac{n_b P_{i,j+1/2} u_{i,j+1/2}}{2\Delta\xi_i h_{1,j+1/2}} - \left[\frac{dn_b}{d\xi}\frac{u_{i,j+1/2} P_{i,j+1/2}(\eta_{n,j+1/2}-1)}{\Delta\eta_{n,j+1} h_{1,j+1/2}} + \frac{V_{i,j+1/2} P_{i,j+1/2}}{\Delta\eta_{n,j+1}}\right]$$

$$B_{NM,j+1/2} = \frac{n_b P_{i,j+1/2} u_{i,j+1/2}}{2\Delta\xi_i h_{1,j+1/2}} + \left[\frac{dn_b}{d\xi}\frac{u_{i,j+1/2} P_{i,j+1/2}(\eta_{n,j+1/2}-1)}{\Delta\eta_{n,j+1} h_{1,j+1/2}} + \frac{V_{i,j+1/2} P_{i,j+1/2}}{\Delta\eta_{n,j+1}}\right]$$

$$C_{NM,j+1/2} = \frac{-(\gamma-1)T_{i,j+1/2}}{\gamma\Delta\eta_{n,j+1}}$$

$$D_{NM,j+1/2} = \frac{(\gamma-1)T_{i,j+1/2}}{\gamma\Delta\eta_{n,j+1}}$$

$$E_{NM,j+1/2} = \frac{n_b P_{i,j+1/2} u_{i,j+1/2}}{2\Delta\xi_i h_{1,j+1/2}}(V_{i-1,j+1} + V_{i-1,j}) - \frac{u^2{}_{i,j+1/2} P_{i,j+1/2}}{h_{1,j+1/2}}(\frac{\partial h_1}{\partial \eta_n})_{j+1/2}$$

7. Nomenclature

- H total enthalpy, $h+V^2/2$
- h static enthalpy, h^*/V_∞^{*2}
- M Mach number
- n normal distance from the shock, n^*/R_n^*
- p Pressure, $p^*/(\rho_\infty^* V_\infty^{*2})$
- Pr Prandtl number, $\mu^* C_p^*/k^*$
- Pr_t turbulent Prandtl number, $\mu_t^* C_p^*/k^*$
- R radius of Curvature
- r radius measured from axis of symmetry, r^*/R_n^*
- S Coordinate measured along the shock wave, S^*/R_n^*
- T temperature, T^*/T_{ref}^*
- T_{ref}^* reference temperature, V_∞^{*2}/C_p^*
- u velocity component tangent to the shock wave, u^*/V_∞^*
- v velocity component normal to the shock wave, v^*/V_∞^*
- Γ_b, Γ_{sh} body and shock angle
- ε Reynolds number parameter, $(\mu_{ref}/\rho_\infty u_\infty R_n)^{1/2}$

ε^+ normalized eddy viscosity, $\mu+/\mu$
η stream function ratio, η/η_{sh}
η_n normalized n Coordinate, $1-n/n_b$
θ accommodation coefficient
κ Curvature, $1/R$
μ dynamic viscosity, μ^*/μ_{ref}^*
ξ normalized S Coordinate, $\xi=S$
ρ density, ρ^*/ρ_∞^*
ψ stream function

Subscripts:
i: Denotes i-th Stream wise Station
j: Denotes j-th Point within Dhock layer
sh: Shock Value
b: Body Valve
n: nose Value
t: turbulent value
w: wall Value
s: Edge of Knudsen layer
∞: Free stream Condition

Superscripts:
* dimensional quantity

8. REFERENCES

[1] C.H.Lewis, "First Order Treatment of Higher-Order Boundary-Layer Effects," The Physics of Fluids, Vol. 13, No. 12, pp. 2939-2949, December 1970,.

[2] M.Mcwherter, R.W.Noack, and W.L.Oberkampf, "Evaluation of Inviscid/Boundary Leyer and Parboiled Navier-Stokes Solutions for Design of Reentry Vehicles," AIAA Paper 84-0486, Jan. 1984.

[3] D.R.Olynick, and S.B.Tiwari, "Navier-Stokes Heating Calculations for Benchmark Thermal Protection System Sizing," Journal of Spacecraft and Rockets, Vol. 33, No. 6, pp. 807-814,Nov. 1996.

[4] B.A.Bhutta, and C.H.Lewis, "Comparison of Hypersonic Experiments and PNS Predictions," Journal of Spacecraft and Rockets, Vol.28, No.4, pp.376-386, July-August 1991.

[5] R.T.Davis, "Numerical Solution of the Hypersonic Viscous Shock Layer Equations," AIAA Fournal, Vol. 8, No. 5, pp. 843-851, May 1970.

[6] K.P.Lee, R.N.Gupta, E.V.Zoby, and J.N.Moss, "Hypersonic Viscous Shock-Layer Solutions Over Long Slender Bodies –Part II: Low Reynolds Number Flow," Journal of Spacecraft and Rockets,Vol.27,No.2,pp.185-193,March-April 1990.

[7] R.Gordon, and R.T.Davis, "An Improved Method For Solving the Viscous Shock Layer Equations," AIAA Journal, Vol. 30, No. 7, July 1992.

[8] J.S.Rayan, J.Flores, and C.Y.Chow, "Development and Validation of a Navier-Stokes Code for Hypersonic External Flows," Journal of Spacecraft and Rockets, Vol. 27, No. 2, , pp. 160-166,1990.

[9] K..Lee, and R.N.Gupta, 'Viscous-Shock-Layer Analysis of Hypersonic Flow Over Long Slender Vehicles," Old Dominion University,Norfolk,Virginia,March 1992.

[10] R.N.Gupta, and E.V.Zoby, " Higher Order Viscous Shock-Layer Solutions for High-Altitude Flows," Journal of Spacecraft and Rockets,Vol.3,No.5,pp.751-758.September-October 1994.

[11] M.J.Werle, B.N.Srivastava, and R.T.Davis, "Numerical Solutions to the Full Viscous Shock Layer Equations using an ADI Technique," Dept. of Aerospace Engineering, univ. of Cincinnati, Cincinnati, OH, Rept. AFL-7-13, 1974.

[12] W.M.Hosney, R.T. Davis, and M.J.Werle, "Improvements to the Solution of Viscous Shock Layer Equations," Arnold Engineering Development Center Report No. TR-79-25, August 1979.

[13] J.D.Waskiewicz, A.L.Murray, and C.H.Lewis, "Hypersonic Viscous Shock layer Flow over a Highly Cooled Sphere Cones," AIAA Journal, Vol. 16, No. 2, pp. 189-192, 1978.

[14] A.L.Murray, and C.H.Lewis, "Hypersonic Three-Dimensional Viscous Shock Layer Flows over Blunt Bodies," AIAA Journal, Vol. 16, No. 12, pp. 1279-1286, 1978.

[15] R.A.Thompson, E.V.Zoby, K.E. Wurster, and P.A.Gnoffo, "An Aero thermodynamic Study of Slender Conical Vehicles," AIAA Paper 87-1475, June 1987.

[16] R.N.Gupta, K.P.Lee, J.N.Moss, E.V.Zoby, and S.N.Tiwari, " Viscous Shock-Layer Analysis of Long Slender Bodies," AIAA Paper 87-2487, Aug. 1987.

[17] R.N.Gupta, K.P.Lee, E.V.Zoby, J.N.Moss, and R.A.Thopson, "Hypersonic Viscous Shock-Layer Solutions over Long Slender Bodies-Part I: High Reynolds Number Flows," Journal of Spacecraft and Rockets, Vol. 27, No. 2, March-April 1990.

[18] B.N.Srivastava, M.J.Werle, and R.T.Davis, "Viscous Shock-Layer Solutions For Hypersonic Sphere Cones," AIAA Journal, Vol. 16, No. 2 ,Feb. 1978.

[19] R.N.Gupta, C.D.Scott, and J.N.Moss, "Slip-Boundary Equations for Multi Component Air Flow," NASA TP 2452, Nor. 1985.

[20] J.N.Moss, "Reacting Viscous-Shock-Layer Solution with Multi Component Diffusion and Mass Injection," NASA TR R-411, Jun. 1974.

[21] B.A.Bhutta, and C.H.Lewis, "Improved Nonequilibrium Viscous Shock-Layer Scheme For Hypersonic Blunt-Body Flow Fields," Journal of Spacecraft and Rockets, Vol. 29, No. 1, Jan. 1992.

[22] S.M.H.Karimian, and A.Mehdizadeh, "Approximate of Inviscid Flow Around the Nose of Hypersonic Bodies at Angle of Attack," Amirkabir Journal, Vol. 12, No. 47, Summer 2001.

[23] T.Cebeci, and A.M.O.Smith, "A Finite-Difference Method For calculating Compressible Laminar and Turbulent Boundary Layers," Journal of Basic Engineering, pp. 523-538, Sep. 1970.

[24] S.Dhawan, and R.Narashima, "Some Properties of Boundary Layer Flow during Transition From Laminar to Turbulent Motion," Journal of Fluid Mechanics, Vol. 1, pp. 418-436, Jan. 1958.

[25] M.Malekzadeh Dirin, M.Maerefat, and S.M.H.Karimian, " Three-Dimensional Approximate Viscous Shock Layer Method For Hypersonic Flow over Blunt Nosed Bosed Bodies," AIAA Paper 2003-0154.

[26] F.M.Cheatwood, and F.R.Dejarnette, "An Approximate Viscous Shock Layer Approach to Cal Culating Hypersonic Flow, about Blunt-Nosed Bodies," AIAA Paper 91-1348, May-June. 1983.

[27] J.W.Cleary, "Effects of Angle of Attack and Bluntbess on Laminar Heating-Rate Distributions of a 15 Degree Cone at a Mach Number of 10.6," NASA TN D-5450, October 1969.

[28] C.G.Miller, "Experimental and Predicted Heating Distributions for Biconics at Incidence in Air at Mach 10," NASA TP-2334, November 1984.

[29] A.K.Sehgal, S.N.Tiwari, and D.J.Singh, "Invistigation of Nose Bluntness and Angle of Attack Effects on Slender Bodies in Viscous Hypertension Flows," Department of Mechanical Engineering and Mechanics, College of Engineering and Technology, Old Dominion University, Norfolk, Virginia, April 30,1991.

[30] D.B.Carver, "Heat Transfer,Surface Pressure and Flow Field Surveys on Conic and Biconic Models with Boundary Layer Trips at Mach 8-Phases IV snf VI," Calspan/Arnold Engineering Development Center Division, Report No. AEDC-TSR-80-V14, March 1980.

[31] D.E.Boylan,,"Laminar Heat Transfer on Sharp and Blunt Ten Degree Cones in Conical and Parallel Low Density Flow," Arnold Engineering Development Center , Tullahama, TN,AEDC-TR-73-106,August 1973.